Available online at www.sciencedirect.com
SCIENCE DIRECT
Remote Sensing of Environment 95 (2005) 480–492
Remote Sensing of Environment
www.elsevier.com/locate/rse

Mapping paddy rice agriculture in southern China using multi-temporal MODIS images

Xiangming Xiao[a,*], Stephen Boles[a], Jiyuan Liu[b], Dafang Zhuang[b], Steve Frolking[a], Changsheng Li[a], William Salas[c], Berrien Moore III[a]

[a]*Institute for the Study of Earth, Oceans and Space, University of New Hampshire, Durham, NH 03824, USA*
[b]*Institute of Geographical Science and Natural Resources, Chinese Academy of Sciences, Beijing 100001, China*
[c]*Applied Geosolutions, LLC., Durham, NH 03824, USA*

Received 8 September 2004; received in revised form 21 December 2004; accepted 24 December 2004

Abstract

Information on the area and spatial distribution of paddy rice fields is needed for trace gas emission estimates, management of water resources, and food security. Paddy rice fields are characterized by an initial period of flooding and transplanting, during which period open canopy (a mixture of surface water and rice crops) exists. The Moderate Resolution Imaging Spectroradiometer (MODIS) sensor onboard the NASA EOS Terra satellite has visible, near infrared and shortwave infrared bands; and therefore, a number of vegetation indices can be calculated, including Normalized Difference Vegetation Index (NDVI), Enhanced Vegetation Index (EVI) and Land Surface Water Index (LSWI) that is sensitive to leaf water and soil moisture. In this study, we developed a paddy rice mapping algorithm that uses time series of three vegetation indices (LSWI, EVI, and NDVI) derived from MODIS images to identify that initial period of flooding and transplanting in paddy rice fields, based on the sensitivity of LSWI to the increased surface moisture during the period of flooding and rice transplanting. We ran the algorithm to map paddy rice fields in 13 provinces of southern China, using the 8-day composite MODIS Surface Reflectance products (500-m spatial resolution) in 2002. The resultant MODIS-derived paddy rice map was evaluated, using the National Land Cover Dataset (1:100,000 scale) derived from analysis of Landsat ETM+ images in 1999/2000. There were reasonable agreements in area estimates of paddy rice fields between the MODIS-derived map and the Landsat-based dataset at the provincial and county levels. The results of this study indicated that the MODIS-based paddy rice mapping algorithm could potentially be applied at large spatial scales to monitor paddy rice agriculture on a timely and frequent basis.

Keywords: Paddy rice fields; MODIS images; Land surface water index; Enhanced vegetation index

1. Introduction

Rice is one of the world's major staple foods and paddy rice fields account for approximately 15% of the world's arable land (IRRI, 1993). A unique physical feature of paddy fields is that the rice is grown on flooded soils. This feature is significant in terms of both trace gas emissions and water resources management. Seasonally flooded rice paddies are a significant source of methane emissions (Denier Van Der Gon, 2000; Li et al., 2002; Neue & Boonjawat, 1998), contributing over 10% of the total methane flux to the atmosphere (Prather & Ehhalt, 2001), which may have substantial impacts on atmospheric chemistry and climate. Agricultural water use (in the form of irrigation withdrawals) accounted for ~70% of global fresh water withdrawals (Samad et al., 1992), and the majority of Asian rice agriculture is irrigated (Huke, 1982; Huke & Huke, 1997). Intensification in rice farming practices in the near future could have significant impacts on the emissions of various greenhouse gases and

* Corresponding author.
E-mail address: xiangming.xiao@unh.edu (X. Xiao).

0034-4257/$ - see front matter © 2005 Elsevier Inc. All rights reserved.
doi:10.1016/j.rse.2004.12.009

availability of water (Li et al., 2002; Wassmann et al., 2000).

Accurate assessment of methane emissions at regional and global scales requires geospatial datasets of paddy rice fields. Several global datasets of paddy rice were developed in the late 1980s and early 1990s (Aselman & Crutzen, 1989; Matthews et al., 1991; Olson, 1992; Wilson & Henderson-Sellers, 1992) and used in global-scale analyses of climate and trace gas emissions. Most of these global datasets have a coarse spatial resolution (from 0.5° to 5° latitude and longitude). Recently, a global cropland data product was developed at a spatial resolution of five arc minutes, which contains a category of paddy rice fields (Leff et al., 2004). At the regional scale, an Asian rice dataset was generated using statistical data of rice agriculture at sub-country administration units from the 1970s, including a base map at a scale of 1:4,500,000 (Huke, 1982). The Asia rice dataset was later updated (Huke & Huke, 1997), using agricultural census data of the sown area of rice agriculture in the early 1990s. This updated Asia rice database was used to estimate methane emissions in Asia (Knox et al., 2000; Matthews et al., 2000). Regional-scale analyses of trace gas emissions, food security, and water resource management require updated datasets of paddy rice fields at a finer spatial resolution.

Optical satellite remote sensing provides a viable means to meet the requirement of improved regional-scale datasets of paddy rice fields. A number of studies have explored the potential of images from Landsat and NOAA Advanced Very High Resolution Radiometer (AVHRR) to identify paddy rice fields (Fang, 1998; Fang et al., 1998; Okamoto & Fukuhara, 1996; Okamoto & Kawashima, 1999; Tennakoon et al., 1992; Van Niel et al., 2003). Those studies that identified rice paddies using fine-resolution Landsat Thematic Mapper (TM) data primarily used image classification procedures. Those studies that used moderate-resolution AVHRR images were primarily based on the temporal development of the Normalized Difference Vegetation Index (NDVI; Eq. (1)) and local knowledge (e.g., crop calendars) of rice paddy fields.

A new generation of advanced optical sensors, including the Moderate Resolution Imaging Spectroradiometer (MODIS) onboard the Terra and Aqua satellites, and VEGETATION (VGT) onboard the SPOT-4 satellite, provide additional shortwave infrared bands that are sensitive to vegetation moisture and soil water. For instance, the VGT sensor has four spectral bands: blue (430–470 nm), red (610–680 nm), near infrared (NIR, 780–890 nm) and shortwave infrared (SWIR, 1580–1750 nm). The availability of an additional SWIR spectral band in VGT provides an opportunity for developing and generating improved vegetation indices that are sensitive to equivalent water thickness (EWT, g H_2O/m^2), such as the Land Surface Water Index (LSWI; Eq. (2)) (Maki et al., 2004; Xiao et al., 2002a, 2002b). During the rice transplanting period and the early part of the rice growing season, paddy fields are a mixture of green rice plants and open water (Xiao et al., 2002d). Recently, we developed an algorithm to identify paddy rice fields, using temporal profiles of LSWI and NDVI data derived from 10-day composite VGT images (Xiao et al., 2002b). Rice paddies were identified as areas where the LSWI values increased (due to the greater surface moisture during the flooding period) and were temporarily greater than NDVI values (Xiao et al., 2002b).

The MODIS sensor has 36 spectral bands, seven of which are designed for the study of vegetation and land surfaces: blue (459–479 nm), green (545–565 nm), red (620–670 nm), near infrared (NIR_1: 841–875 nm; NIR_2: 1230–1250 nm), and shortwave infrared ($SWIR_1$: 1628–1652 nm, $SWIR_2$: 2105–2155 nm). Daily global imagery is provided at spatial resolutions of 250-m (red and NIR_1) and 500-m (blue, green, NIR_2, $SWIR_1$, $SWIR_2$). The MODIS Land Science Team provides a suite of standard MODIS data products to the users, including the 8-day composite MODIS Surface Reflectance Product (MOD09A1). Compared to the 10-day composite VGT product, the 8-day composite MODIS data have three advantages for paddy rice analyses: (a) finer spatial resolution (500 m versus 1 km in VGT), (b) slightly shorter temporal resolution (8-day in MODIS versus 10-day in VGT), and (c) improved atmospheric correction (Vermote & Vermeulen, 1999).

The objective of this study is to assess the potential of MODIS images for identifying inundation and paddy rice fields. Southern China was selected as the case study area for MODIS-based large-scale mapping of paddy rice fields because it has a large amount of paddy rice agriculture and fine-resolution cropland area reference data are available for the evaluation of MODIS-based results (Frolking et al., 1999, 2002; Xiao et al., 2003b). If successful, the algorithm we developed for MODIS images can be applied to other rice-producing countries in Asia to generate an updated continental database of paddy rice agriculture; such a product would support various analyses that address biogeochemical nutrient cycling, trace gas emissions, water management, food security, agricultural vulnerability and sustainability.

2. Study area, data and methods

2.1. Description of the study area

There are large spatial variations in agriculture and crop rotation systems in China (Frolking et al., 2002; Qiu et al., 2003). In this study we focused on 13 provincial-level administrative units (12 provinces plus Shanghai) in southern China (Fig. 1), which represent over 2.5 million km^2 of land area (Table 1). Two-crop rotation systems are dominant across southern China, because of a long warm season and abundant precipitation (Frolking et al., 2002; Qiu et al.,

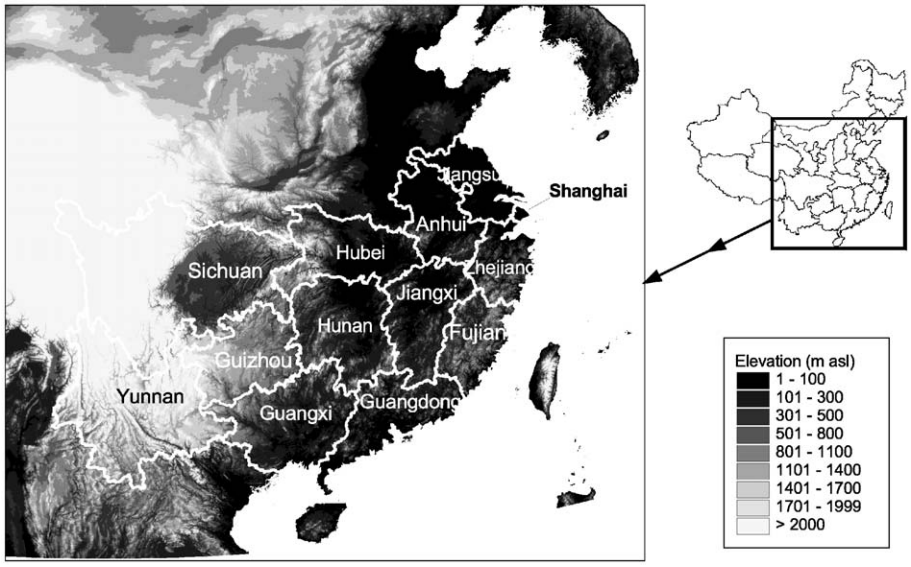

Fig. 1. Digital elevation model (DEM) of southern China (http://edc.usgs.gov/products/elevation/gtopo30.html). The study area covers 13 provinces in southern China.

2003). A rotation of upland (e.g., winter wheat, rapeseed) and paddy rice crops occurs mostly in the northern part of the study area (e.g., Jiangsu province), where the landscape is very flat and land cover is relatively homogenous, dominated by cropland. In the western and southern parts of the study area, a rotation of early rice and late rice crops occurs, but the fraction of the landscape allocated to croplands is generally much less than in the northern part of the study area. Land cover types in those areas are more heterogeneous and influenced by increased complexity of topography, and represent a mixed landscape of cropland and forest.

Table 1
A summary of land area, paddy rice agriculture and upland cropland from the National Land Cover Dataset (NLCD-2000) for the 13 provincial administrative units in southern China

Province	Land area (km^2)	Area of upland cropland (km^2)	Area of paddy rice (km^2)	Percent of rice area with ≥20% fractional cover in 1-km pixels	Median percent of paddy rice within 1-km pixels
Jiangsu	100,857	18,325	32,022	98	62
Anhui	140,210	28,500	31,879	94	60
Sichuan	567,092	74,710	39,708	79	33
Shanghai	6689	338	2888	98	31
Hubei	185,968	21,982	28,518	85	43
Zhejiang	101,945	3434	17,800	87	52
Hunan	211,964	11,036	32,348	80	37
Jiangxi[a]	167,651	9032	24,250	78	36
Fujian[a]	121,685	4332	10,590	69	29
Guizhou[a]	176,183	26,191	11,144	67	27
Yunnan[a]	384,281	34,892	11,955	78	37
Guangxi[a]	236,359	12,425	18,683	75	36
Guangdong[a]	177,316	9644	18,769	80	38
Total	2,578,198	254,841	280,555	86	43

[a] "Hilly" provinces.

2.2. MODIS image data

Among a suite of standard MODIS data products available to the users, we used the 8-day composite MODIS Surface Reflectance Product (MOD09A1). Each 8-day composite includes estimates of surface spectral reflectance of the seven spectral bands at 500-m spatial resolution. In the production of MOD09A1, atmospheric corrections for gases, thin cirrus clouds and aerosols are implemented (Vermote & Vermeulen, 1999). The 8-day composite product is generated through a multi-step process that first eliminates observations with a low quality score or low observational coverage, and then selects the observation with the minimum value of blue band (band 3) during the 8-day composite period (http://modis-land.gsfc.nasa.gov/MOD09/MOD09ProductInfo/MOD09_L3_8-day.htm). The composites still have reflectance variations associated with variation in the bidirectional reflectance distribution function (BRDF). MOD09A1 also includes quality control flags to account for various image artifacts (e.g., clouds, cloud shadow). MODIS products are organized in a tile system with the Sinusoidal (SIN) projection grid, and each tile covers an area of 1200 km by 1200 km (approximately 10° latitude by 10° longitude at equator). In this study, we downloaded MOD09A1 data for 2002 (forty-six 8-day composites) from the USGS EROS Data Center (http://edc.usgs.gov/). Six tiles (H26V05, H26V06, H27V05, H27V06, H28V05 and H28V06) are needed to cover the study area of southern China (Fig. 1).

2.3. Calculation of vegetation indices

For each 8-day composite, we calculated NDVI, LSWI and Enhanced Vegetation Index (EVI; Eq. (3)) (Huete et al.,

1997), using surface reflectance values from the blue, red, NIR (841–875 nm) and SWIR (1628–1652 nm) bands:

$$\mathrm{NDVI} = \frac{\rho_{\mathrm{nir}} - \rho_{\mathrm{red}}}{\rho_{\mathrm{nir}} + \rho_{\mathrm{red}}} \quad (1)$$

$$\mathrm{LWSI} = \frac{\rho_{\mathrm{nir}} - \rho_{\mathrm{swir}}}{\rho_{\mathrm{nir}} + \rho_{\mathrm{swir}}} \quad (2)$$

$$\mathrm{EVI} = 2.5 \times \frac{\rho_{\mathrm{nir}} - \rho_{\mathrm{red}}}{\rho_{\mathrm{nir}} + 6 \times \rho_{\mathrm{red}} - 7.5 \times \rho_{\mathrm{blue}} + 1} \quad (3)$$

While NDVI is correlated to the leaf area index (LAI) of paddy rice fields (Xiao et al., 2002d), it has some limitations, including saturation under closed canopy and sensitivity to atmospheric conditions and soil background (Huete et al., 2002; Xiao et al., 2003a). The blue band is sensitive to atmospheric conditions and is used for atmospheric correction. EVI directly adjusts the reflectance in the red band as a function of the reflectance in the blue band, and it accounts for residual atmospheric contamination (e.g., aerosols) and variable soil and canopy background reflectance (Huete et al., 1997, 2002). In addition to NDVI, we have explored the biophysical performance of EVI and LSWI and their potential for land cover classification (Boles et al., 2004; Xiao et al., 2002a, 2002c).

2.4. Algorithms for identifying inundation and paddy rice field

A unique physical feature of paddy rice fields is that rice plants are grown on flooded soils. Temporal dynamics of paddy rice fields can be characterized by three main periods: (1) the flooding and rice transplanting period; (2) the growing period (vegetative growth, reproductive and ripening stages); and (3) the fallow period after harvest (Le Toan et al., 1997). During the flooding and rice transplanting period, the land surface is a mixture of surface water and green rice plants (Xiao et al., 2002b). Water depth generally varies from 2 to 15 cm. About 50 to 60 days after transplanting, rice plant canopies cover most of the surface area. At the end of the growth period prior to harvesting (the ripening stage), there is a decrease of leaf and stem moisture content and a decrease of the number of green leaves.

For optical sensors, detection of changes in the mixture of surface water and green vegetation in paddy rice fields requires spectral bands or vegetation indices that are sensitive to both water and vegetation. In an earlier study, we examined the potential of a greenness-related vegetation index (NDVI) and a water-related vegetation index (LSWI) for identifying flooding and rice transplanting in eastern Jiangsu Province, China (Xiao et al., 2002b), where agriculture is dominated by a rotation of two seasonal crops (winter wheat or rapeseed crops followed by paddy rice). LSWI temporal dynamics were variable enough to capture substantial increases of surface water due to flooding (inundation) and rice transplanting at paddy rice fields. Using multi-temporal 10-day composites from the VGT sensor, a temporal profile analysis of both NDVI and LSWI was conducted to identify the period of flooding and rice transplanting at paddy rice fields using a simple threshold assumption, i.e., LSWI>NDVI (Xiao et al., 2002b). In that earlier study, field observations on crop rotation, LAI, water management and fertilizer application at five field sites were conducted (Xiao et al., 2002b, 2002d). The paddy rice mapping algorithm was applied and evaluated in eastern Jiangsu Province with an area of 175×165 km^2 (Xiao et al., 2002b).

In this study we continued to explore the algorithm that combines NDVI and LSWI (Xiao et al., 2002b), while also including EVI into the analysis. We examined temporal profiles of MODIS-based vegetation indices for the same five field sites in Jiangsu province as reported in an earlier study (Xiao et al., 2002b). As illustrated at one of the five field sites, EVI values in croplands were generally larger than LSWI values throughout much of the year. However, LSWI values were slightly higher than EVI in late June of 2002 (Fig. 2). According to field observations in 1999–2000 at this site, crop cultivation in this site shifted from winter wheat (non-flooded) to paddy rice (flooded) in late June (Xiao et al., 2002b). For the other four field sites (not shown here), there were MODIS-based observations that had either EVI<LSWI or NDVI<LSWI in one to a few 8-day composites, which are consistent with the observations reported in an earlier study that used 10-day VGT composite data (Xiao et al., 2002b).

Individual farmers have different flooding and rice transplanting schedules for their paddy rice fields, which poses a great challenge for remote sensing analyses at large spatial scales. Our hypothesis is that a temporary inversion

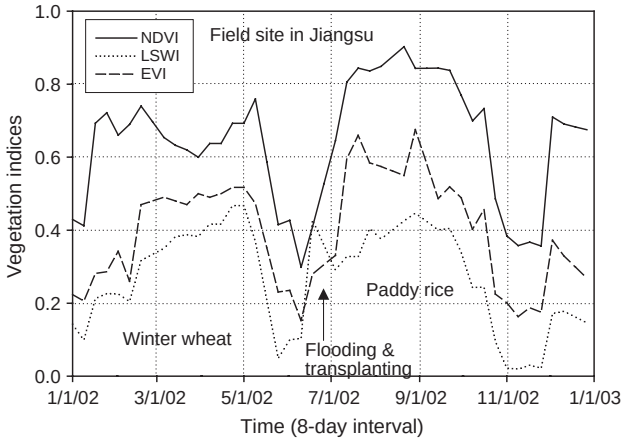

Fig. 2. The seasonal dynamics of the Normalized Difference Vegetation Index (NDVI), the Enhanced Vegetation Index (EVI), and the Land Surface Water Index (LSWI) at a field site in Jiangning County (south of Nanjing), Jiangsu Province. This site (118°54.519′ E, 31°49.623′ N) has winter wheat crops in winter/spring seasons and paddy rice in summer/fall seasons. Harvest of winter wheat crops usually takes place in early- to mid-June, and flooding and rice transplanting usually take place in mid- to late-June (Xiao et al., 2002b).

of the vegetation indices, where LSWI either approaches or overtakes NDVI or EVI values, may signal flooding and rice transplanting in paddy rice fields. To slightly relax the assumption (LSWI>NDVI) used in the earlier study (Xiao et al., 2002b), we used the following thresholds for identifying a flooded/transplanting pixel: LSWI+0.05≥NDVI or LSWI+0.05≥EVI. After a pixel was identified as a "flooding and transplanting" pixel, a procedure was implemented to determine whether rice growth occurs in that pixel, using the assumption that the EVI value of a true rice pixel reaches half of the maximum EVI value (in that crop cycle) within five 8-day composites (40-days) following the date of flooding and transplanting. Rice crops grow rapidly after transplanting, and LAI usually reaches its peak within 2 months (Xiao et al., 2002d).

2.5. Regional implementation of algorithms

To implement the MODIS rice detection algorithm at the regional scale is a challenging task, as many factors could potentially affect the seasonal dynamics of vegetation indices, including snow cover, clouds, water bodies and other vegetation background. Implementation of the algorithm over a large and complex spatial domain requires careful consideration of those factors. Therefore, we developed a procedure for regional implementation of the algorithm by generating various masks for clouds, snow cover, water bodies, and forest cover in an effort to minimize their potential impacts (Fig. 3).

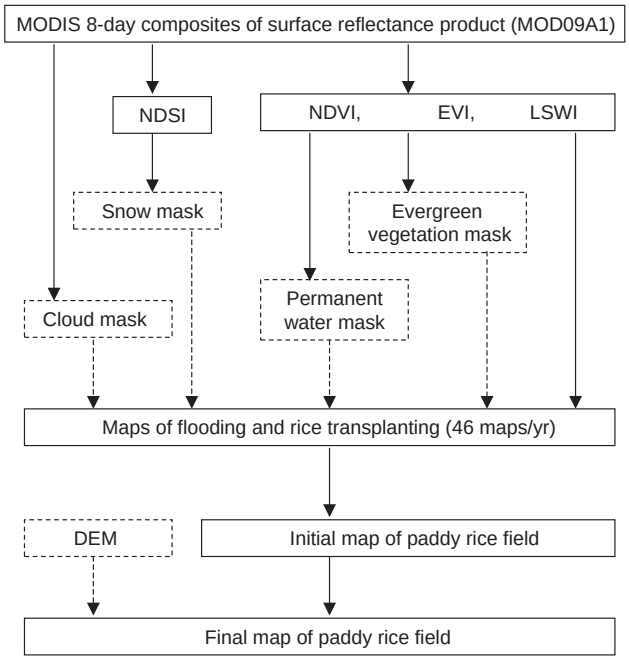

Fig. 3. A schematic diagram illustrating the algorithms for large-scale mapping of flooding and paddy rice fields from MODIS 8-day surface reflectance images at 500-m spatial resolution. One year of 8-day MODIS surface reflectance data (a total of forty-six 8-day composites) are used as input data.

The MOD09A1 file includes quality control flags for clouds. We extracted the information on clouds and generated masks of cloud cover for all time periods of each MODIS tile. It was noticed that a number of pixels had a high blue band reflectance but were not labeled as clouds in the MOD09A1 cloud quality flag. These pixels tended to have high LSWI relative to NDVI and EVI, potentially resulting in false identification of paddy rice areas. An additional restriction was then applied, whereas pixels with a blue reflectance of ≥0.2 were also masked as cloudy pixels. For each MODIS tile, 46 cloud cover maps were generated; all cloud observations were excluded from further analyses.

Snow cover has large surface reflectance values in the visible spectral bands and could potentially affect vegetation index values. To minimize the potential impact of those areas with snow cover in winter and spring on our analysis, we used the snow cover algorithms developed for the MODIS snow product (Hall et al., 1995, 2002) to generate snow cover masks. Normalized Difference Snow Index (NDSI; Eq. (4)) was first calculated for each 8-day composite, using surface reflectance values from the green and NIR bands; and then thresholds (NDSI>0.40 and NIR>0.11) were applied to identify snow-covered pixels. For each MODIS tile, 46 snow cover maps were generated and then merged into one mask of snow cover, which counts the number of 8-day periods a pixel was classified as snow. Pixels containing snow at any time during the year were excluded for the identification of flooding and rice transplanting.

$$\mathrm{NDSI} = \frac{\rho_{\mathrm{green}} - \rho_{\mathrm{nir}}}{\rho_{\mathrm{green}} + \rho_{\mathrm{nir}}} \tag{4}$$

There is also a need to separate persistent water bodies from seasonally flooded pixels (e.g., paddy rice). Instead of using conventional image classification approach (e.g., cluster analysis of forty-six 8-day composites) to generate a mask of persistent water bodies, we developed a simple method that is based on temporal dynamics of NDVI and LSWI. We first analyzed temporal profiles of NDVI and LSWI, and assumed a pixel to be covered by water if NDVI<0.10 and NDVI<LSWI, and generated a map that counts the number of 8-day periods within the year to be classified as water. Second, we assumed a pixel to be persistent water bodies if it was identified as water in ten or more 8-day composite periods in the year. Since the flooding/transplanting period is temporary, flooded rice pixels are expected to have fewer than ten composite periods classed as water. Those pixels identified as persistent water bodies were excluded from calculation of the flooding map. For each MODIS tile, one mask of permanent water bodies was generated.

To further avoid confusion from flooded natural vegetation, we have constructed a mask of natural evergreen vegetation, using a two-test procedure that employed both

NDVI and LSWI time series data. Natural evergreen vegetation in southern China is generally composed of evergreen trees or shrubs. The first test was designed to identify evergreen forests. Evergreen forest areas tend to have a long and consistently high NDVI value throughout a year, while cropland (e.g., rice) pixels tend to have only a few 8-day periods with high NDVI values, just prior to harvesting. Evergreen forest pixels were identified as those pixels having NDVI values of ≥0.7 over at least twenty 8-day composites during the year. Since the NDVI forest restriction is a *cumulative* count, we used a gap-filled product that corrects NDVI values in the time series where the cloud mask indicated clouds (Xiao et al., 2002b). The second test was designed to identify evergreen shrubland/woodland/grassland, which generally have much lower leaf area index or NDVI values than evergreen forests. Croplands usually have some periods of time with exposed soils (e.g., after-harvest or land preparation), when LSWI values are very low with exposed soils and crop litterfall. After examining the seasonal dynamics of LSWI for various vegetation types in southern China, we found out that permanently vegetated areas (with green vegetation throughout a year) rarely have a LSWI value of <0.15. In this study we simply assign those pixels with no LSWI value of <0.15 during a year to be natural evergreen vegetation. For each MODIS tile, one mask of natural evergreen vegetation was generated, and those pixels of evergreen vegetation were excluded from identification of flooding and paddy rice fields.

While much of the rice agriculture in southern China occurs in great flat plains near the mouth of the Yangtze River, there is some significant topography in the far south and west of the study area that could pose challenges to the development of a rice detection algorithm. The digital elevation model (GTOPO30; Global 30-Arc Second Elevation Dataset; http://edc.usgs.gov/products/elevation/gtopo30.html) was acquired and we calculated slope of pixels, using the Arc/Info software. We compared the elevation map and slope map with the paddy rice map from the NLCD-2000 dataset (see Section 2.5 for details). Few pixels with a large fraction of paddy rice occur at an elevation >2000 m and/or a slope of ≥2°. Therefore, we generated a DEM mask and used it to exclude those areas above 2000 m in elevation and with a slope greater than 2°. Based on a qualitative assessment of topographical characteristics, provinces were roughly separated as primarily 'flat' (Jiangsu, Anhui, Sichuan, Shanghai, Hubei, Zhejiang, Hunan) or 'hilly' (Fujian, Guizhou, Jiangxi, Yunnan, Guangxi, Guangdong) so that the potential impacts of topography on the performance of the MODIS-based paddy rice detection algorithm could be explored.

For each 8-day composite, we compared NDVI, EVI and LSWI values and generated the maps of "flooding and transplanting" pixels, based on our hypothesis that a temporary inversion of the vegetation indices (LSWI+0.05≥EVI or LSWI+0.05≥NDVI) may signal flooding and rice transplanting in paddy rice fields. Flooded pixels were mapped if LSWI+0.05≥EVI or LSWI+0.05≥NDVI occurred in any one composite of the time series. Pixels that had previously been identified as water, snow, cloud, forest, or natural evergreen vegetation were masked out from this analysis. For each MODIS tile, 46 maps of flooded pixels were generated. For each pixel that was identified as a flooded pixel in one or more 8-day periods, we examined the time-series of EVI in a year. A procedure was implemented to identify rice growth, using the criteria that the EVI value reached half of the maximum EVI value (in that crop cycle) within five 8-day periods (40 days) after flooding was identified.

We computed vegetation indices, masks, flooding maps and rice maps for the six individual MODIS tiles that cover southern China. We then mosaicked all rice map tiles, and re-projected the resultant map into Lambert Azimuthal Equal Area projection. An administrative boundary map (both provincial- and county-level at the scale of 1:1,000,000) of China was used to generate summaries of rice area at both provincial and county levels.

2.6. Ancillary data for evaluation of MODIS-based analysis

Accuracy assessment of moderate-resolution (500 m–1 km) land cover products is a challenging task, as these maps can overestimate or underestimate areas of individual land cover types due to the fragmentation and sub-pixel proportion of individual land cover types. Because of budget constraints and human resource limitations, we were not able to conduct extensive field surveys for collecting site-specific data. As an alternative approach to field surveys, we used fine-resolution images and derived land cover maps to evaluate the MODIS-derived rice maps. In this study, validation of the MODIS-derived paddy rice map was performed using detailed land cover datasets derived from fine-resolution Landsat data.

The National Land Cover Project (NLCD), under the support of the Chinese Academy of Sciences, completed the analysis of Landsat 7 Enhanced Thematic Mapper (ETM+) images acquired in 1999 and 2000 for all of China (Liu et al., 2003). 508 ETM+ images in 1999/2000 were geo-referenced and ortho-rectified, using field collected ground control points and fine-resolution digital elevation models. A classification system of 25 land cover types was used in the NLCD project, including "paddy rice" and "upland cropland" categories. Visual interpretation of ETM+ images was conducted to generate a thematic map of land cover in China at a scale of 1:100,000. The resultant vector dataset was converted into a gridded database at 1-km spatial resolution. The 1-km gridded database still captures all of the land cover information at the 1:100,000 scale by calculating the percent fractional cover within a 1-km pixel for individual land cover types (Xiao et al., 2002c). The 1-km resolution gridded "paddy rice" layer of the NLCD dataset (hereafter referred to as NLCD-2000) was used for

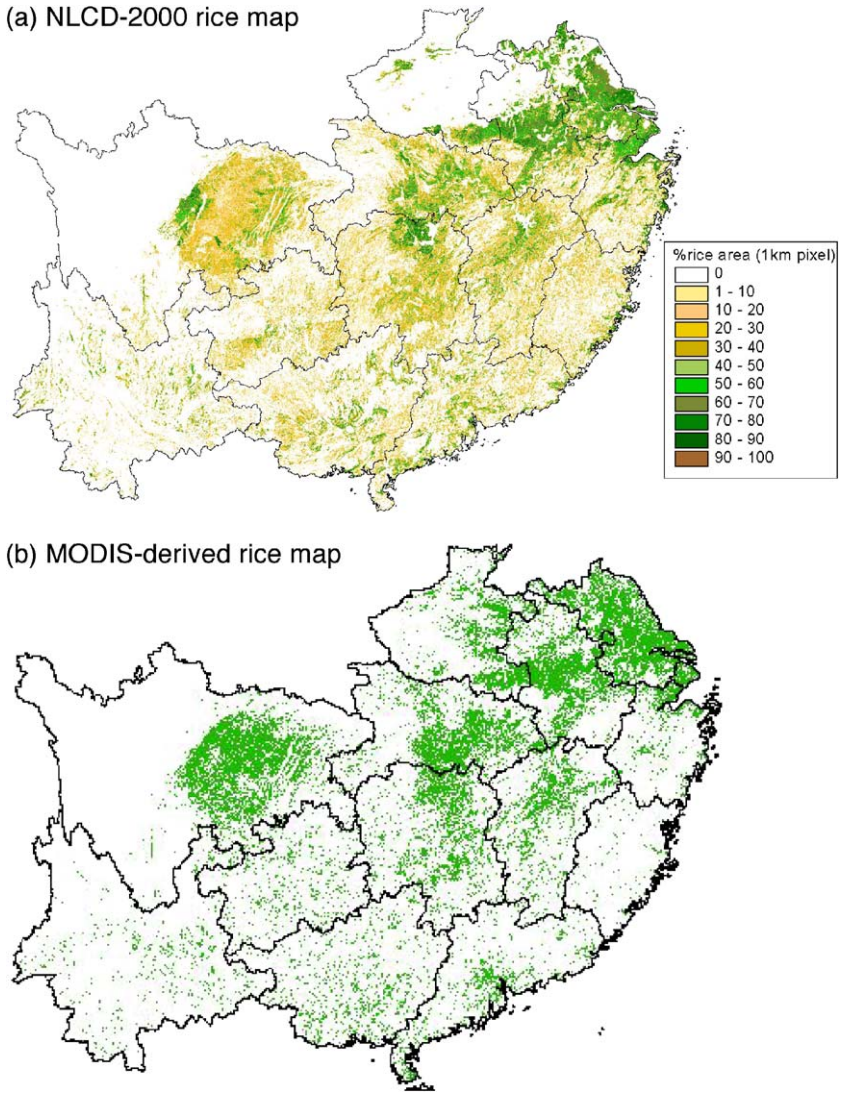

Fig. 4. Spatial distribution of paddy rice fields in southern China, as derived from (a) the NLCD-2000 database (Liu et al., 2003), and (b) the analysis of MODIS 8-day surface reflectance data (at 500-m spatial resolution) in 2002.

evaluation of MODIS-based rice maps (Fig. 4a). According to the NLCD-2000 dataset, there is a total of 280,555 km^2 area of "paddy rice" and 254,841 km^2 area of "upland crops" in the 13 provincial administrative units, respectively, accounting for 21% of total land area in the study region (Table 1).

3. Results

3.1. Spatial distribution of paddy rice in southern China from MODIS-derived rice map

Fig. 4b shows the spatial distribution of paddy rice in southern China derived from MODIS data in 2002 (hereafter referred to as MOD_{rice}). Paddy rice agriculture occurred throughout most of the study area, with the exception of western Sichuan where altitude and topography prohibit rice growth. Rice agriculture was concentrated in major lake regions (Tai Lake in Jiangsu, Poyang Lake in Jiangxi, Dongting Lake in Hunan), the middle and lower reaches of the Yangtze River, and large plains (e.g., Chendu Plain in Sichuan). Rice agriculture occurred more sporadically in the southern portion of the study area, where increased complexity of topography restricts the size of rice fields that can occur. The heterogeneous land cover in these areas is generally a mix of cropland and forest, with most of the rice agriculture occurring in smaller river valleys or on terraced slopes.

The spatial pattern of paddy rice from MOD_{rice} (Fig. 4b) is generally similar to that of the NLCD-2000 reference dataset (Fig. 4a). There were some notable differences between the MOD_{rice} map and the NLCD-2000 reference rice map. First, in northern Jiangsu and most of Sichuan, MOD_{rice} identified paddy rice fields while the NLCD-2000 product had lower fractional amounts of rice fields. Second,

in Fujian province the NLCD-2000 product has a relatively even distribution of rice fields with low fractional coverage, while the MOD_{rice} greatly underestimated rice area in this province (Table 2).

3.2. Quantitative evaluation of MODIS-derived rice map

Certain challenges arise when using a fractional cover dataset that was derived from fine-resolution imagery (e.g., Landsat ETM+) to validate a moderate spatial resolution per-pixel (0 or 1 binary set) dataset (e.g., MOD_{rice}). One has to choose an appropriate threshold of percentage fractional cover of the reference dataset for validation purposes, as it is not reasonable to assume that a moderate resolution product will detect those pixels that have only small percentages of paddy rice fields. The definition of this minimal fractional coverage is important to the validation results, and it is dependent upon the pixel size of both NLCD-2000 (1 km) and MOD_{rice} (500 m). According to the NLCD2000 dataset, there was a total area of 280,555 km^2 paddy rice in the 13 provinces of southern China (Table 1). We calculated the frequency distribution of paddy rice fields within 1-km pixels in the NLCD-2000 dataset by province, and the cumulated frequency graphs show large differences among provinces in southern China (Fig. 5). In those seven provinces dominated by relative flat plains (top graph), a large portion of pixels tend to have high percentage fractions of paddy rice fields (Fig. 5). The total area of paddy rice in those seven flat provinces is about 185,164 km^2, accounting for 66% of total paddy rice area in the 13 provinces of southern China. The median point (50% of pixels) for the fractions of paddy rice within 1-km pixels varies from 27% in Guizhou province to 62% in Jiangsu province (Table 1).

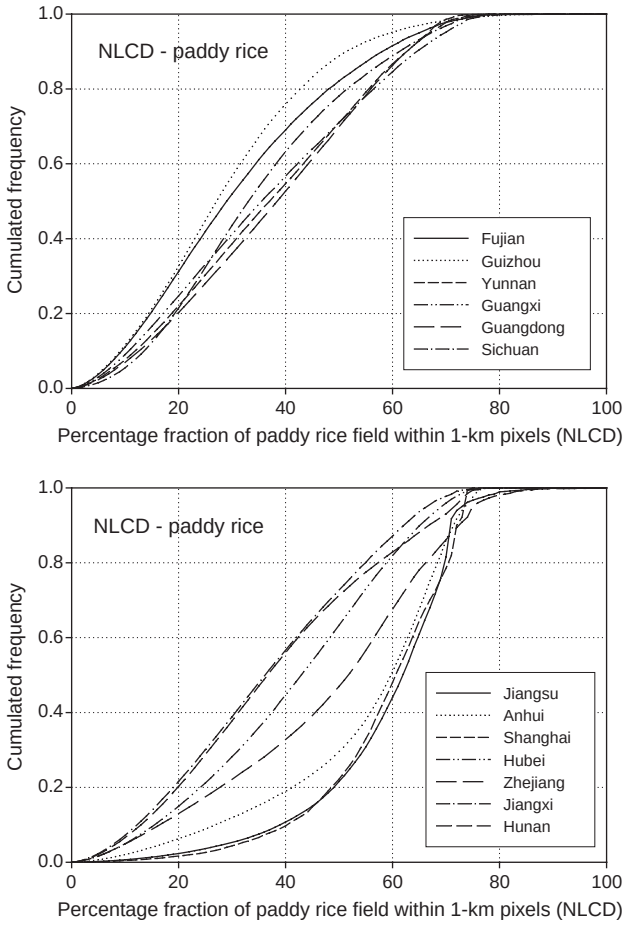

Fig. 5. Histograms of paddy rice fields within 1-km NLCD-2000 pixels by provinces in southern China. The cumulated frequency is used in the graph.

Table 2
Spatial agreements between MOD_{rice} and $NLCD_{20}$ paddy rice pixels by provinces

Province	Both MOD_{rice} and $NLCD_{20}$	MOD_{rice} only	$NLCD_{20}$ only	Spatial agreement (%) using $NLCD_{20}$ or MOD_{rice} as basis	
				$NLCD_{20}$	MOD_{rice}
Jiangsu	40,856	17,517	14,737	73	70
Anhui	35,320	13,342	21,507	62	73
Sichuan	47,941	40,038	40,589	54	54
Shanghai	3929	589	1122	78	87
Hubei	31,925	18,053	26,953	54	64
Zhejiang	11,634	2296	21,299	35	84
Hunan	30,386	15,020	37,312	45	67
Jiangxi	21,675	9197	28,792	43	70
Fujian	1901	2183	19,277	9	47
Guizhou	3414	11,692	20,073	15	23
Yunnan	5495	11,241	18,899	23	33
Guangxi	7323	17,504	29,398	20	29
Guangdong	8680	11,420	29,819	23	43
Total	250,480	170,092	309,778	45	60

In a two-way table, we calculated the sum of Column #2 and Column #3 (MOD_{sum}) and the sum of Column #2 and Column #4 ($NLCD_{sum}$), and then calculated the spatial agreements (%): $NLCD_{20}$ (Column #5)=Column #2/$NLCD_{sum}$, and MOD_{rice} (Column #6)=Column #2/MOD_{sum}.

Note that a MODIS pixel in the MOD09A1 product has a spatial resolution of 463-m×463-m and an area of 214,369 m^2, being about 21% of 1-km pixel area (1,000,000 m^2) of the NLCD-2000 data. In this study we designated those pixels in the NLCD-2000 dataset with a fractional coverage of ≥20% paddy rice as paddy rice pixels, and generated a binary (0 or 1) map of paddy rice fields (hereafter $NLCD_{20}$). The total area of paddy rice from all the NLCD pixels with a fraction of ≥20% paddy rice is about 241,193 km^2 (Table 3), accounting for 86% of the total paddy rice area (280,555 km^2) in Southern China. To compare the MOD_{rice} map and the $NLCD_{20}$ reference rice map at administrative units (province and county), administrative boundaries of China were overlaid with the paddy rice maps to calculate the total rice area for the 13 provinces and 1153 counties in the study area. The spatial agreement between MOD_{rice} and $NLCD_{20}$ has a strong topographic bias, varying between 78% in a flat province (Shanghai) and 9% in a hilly province (Fujian), respectively (Table 2). A number of factors could result in the MOD_{rice} pixels that do not correspond spatially with $NLCD_{20}$ pixels, including falsely identified rice pixels in the

Table 3
A provincial-level comparison of area estimates of paddy rice field (km^2) from MODIS 8-day surface reflectance data and the National Land Cover Dataset (NLCD) from 1999/2000 (Liu et al., 2003)

Province	Pixel-based comparison paddy rice area (km^2) with an assumption of 100% fraction		Fractional area-based comparison paddy rice area (km^2) with fractional values from NLCD	
	MOD_{rice}	$NLCD_{20}$	$MOD_{rice(area)}$	$NLCD_{20(area)}$
Jiangsu	58,373	55,593	40,856	31,276
Anhui	48,663	56,827	35,320	29,867
Sichuan	87,979	88,530	47,941	31,192
Shanghai	4518	5051	3929	2840
Hubei	49,977	58,878	31,924	24,252
Zhejiang	13,930	32,933	11,634	15,488
Hunan	45,406	67,698	30,386	25,801
Jiangxi	30,872	50,467	21,675	19,024
Fujian	4084	21,179	1901	7284
Guizhou	15,106	23,487	3414	7507
Yunnan	16,736	24,394	5495	9321
Guangxi	24,827	36,721	7323	14,070
Guangdong	20,100	38,500	8680	14,972
Total	420,572	560,257	250,480	241,193

We assigned those NLCD pixels that have at least 20% rice coverage within 1 km as paddy rice pixels ($NLCD_{20}$). $MOD_{rice(area)}$ is calculated as the sum of fractions of paddy rice in the NLCD dataset for all the MODIS paddy rice pixels. $NLCD_{20(area)}$ was calculated as the sum of fractions of paddy rice in the NLCD dataset for all the $NLCD_{20}$ paddy rice pixels.

MOD_{rice} product or errors in the $NLCD_{20}$ product. For example, in the process of Landsat image classification, image interpreters may have had the difficult choice of labeling a cropland as either paddy rice field or upland crop field in a system of double cropping (e.g., a rotation of winter wheat and paddy rice).

We conducted two sets of comparisons between MOD_{rice} and $NLCD_{20}$ maps. The first comparison is to mimic a pixel-based comparison by assuming all MODIS-based paddy rice pixels and $NLCD_{20}$ paddy rice pixels have 100% fractional cover of paddy rice within individual pixels. In the pixel-based comparison, the correlations in the area estimates between MOD_{rice} and $NLCD_{20}$ at the provincial level were high, with r^2=0.88 for flat provinces and r^2=0.80 for hilly provinces (Fig. 6). While caution should be used when deriving correlation coefficients from samples with a small population (e.g., number of provinces),

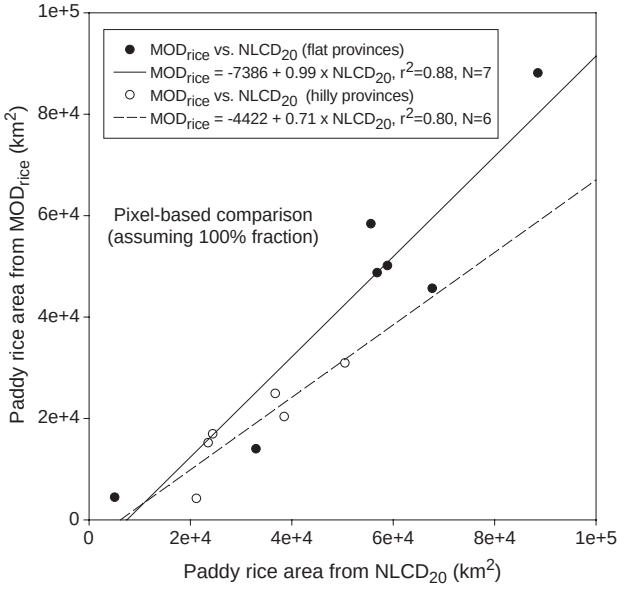

Fig. 6. Province-level, per-pixel comparisons of paddy rice fields in southern China between the MODIS rice algorithm (MOD_{rice}) and NLCD-2000 dataset. Province-level results were analyzed using a pixel-based comparison approach, in which we assumed that all MOD_{rice} pixels and the $NLCD_{20}$ paddy rice pixels have 100% fractional cover of paddy rice.

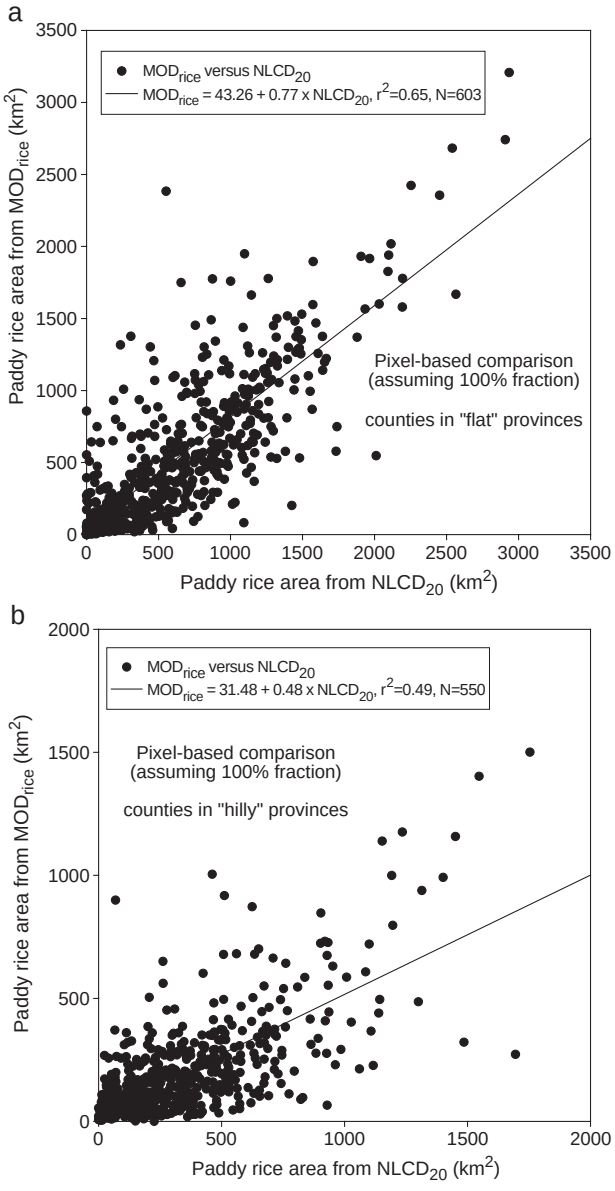

Fig. 7. County-level, per-pixel comparisons of paddy rice fields in southern China between the MODIS rice algorithm (MOD_{rice}) and NLCD-2000 dataset. County-level results were analyzed using a pixel-based comparison approach, in which we assumed that all MOD_{rice} pixels and the $NLCD_{20}$ paddy rice pixels have 100% fractional cover of paddy rice.

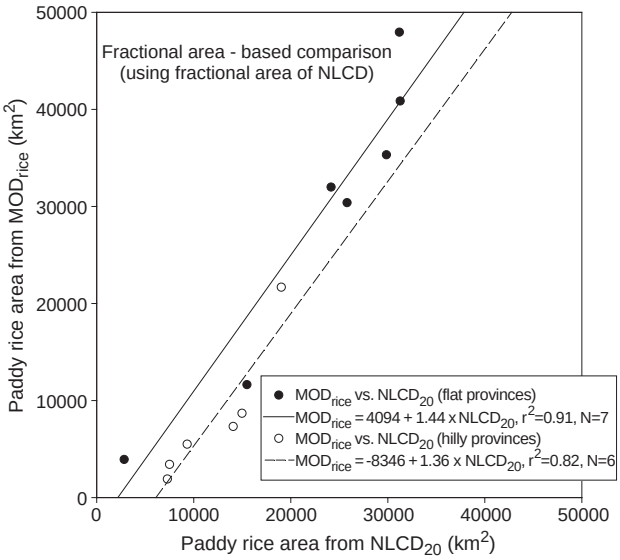

Fig. 8. Province-level comparisons of area estimates of paddy rice fields in southern China between the MODIS rice algorithm (MOD_{rice}) and NLCD-2000 dataset. Province-level results were analyzed using a fractional area-based comparison approach, in which we used the fractional area of paddy rice within individual pixels from the NLCD data for all MOD_{rice} pixels and $NLCD_{20}$ paddy rice pixels.

the root mean square error (RMSE) is an alternative statistical measure that can be used to compare the datasets. The RMSE were 14,492 km^2 for hilly provinces and 11,909 km^2 for flat provinces, respectively (Fig. 6). The area estimates of MOD_{rice} were lower than the areas of $NLCD_{20}$ for all provinces except Jiangsu (Table 3). This underestimation by the MOD_{rice} product becomes more pronounced outside of the lower reaches of the Yangtze River. The impact of topography was evident when comparing the rice area estimates in both flat and hilly provinces. In the flat provinces, the average provincial area of MOD_{rice} was 79.4% of the $NLCD_{20}$ total, but in hilly provinces the average provincial area of MOD_{rice} was only 55% of the $NLCD_{20}$. The reason for MOD_{rice} to underestimate rice areas in the hilly provinces is likely a result of smaller rice field sizes in this part of the study area (Fig. 5), and complex patterns of simultaneous harvesting and rice transplanting in the fields.

In the pixel-based comparison, the correlations in the area estimates between MOD_{rice} and $NLCD_{20}$ at the county level also varied between the flat provinces and the hilly provinces (Fig. 7). For those counties within the flat provinces (Fig. 7a), there was a correlation (r^2=0.65, RMSE=327 km^2) between MOD_{rice} and $NLCD_{20}$, although it was not as strong as was encountered at the provincial level (Fig. 6). For those counties within hilly provinces (Fig. 7b), the correlation between MOD_{rice} and $NLCD_{20}$ is lower (r^2=0.49, RMSE=263 km^2), but still positive.

The second comparison, the fractional area-based comparison, directly uses the fractional values of paddy rice in the NLCD dataset to calculate the areas for all the MODIS-based paddy rice pixels. In the fractional area-based comparison, there were strong linear relationships in area estimates of paddy rice at the province level between MOD_{rice} and $NLCD_{20}$ (Fig. 8), with RMSE=8434 km^2 for flat provinces and RMSE=5041 km^2 for hilly provinces. However, the actual area estimates that are compared in this validation exercise show a strong topographical effect. With the exception of Zhejiang Province, the rice area of all the flat provinces was overestimated by MOD_{rice} compared to $NLCD_{20}$ fractional area, while all of the hilly provinces were underestimated by MOD_{rice} (Table 3).

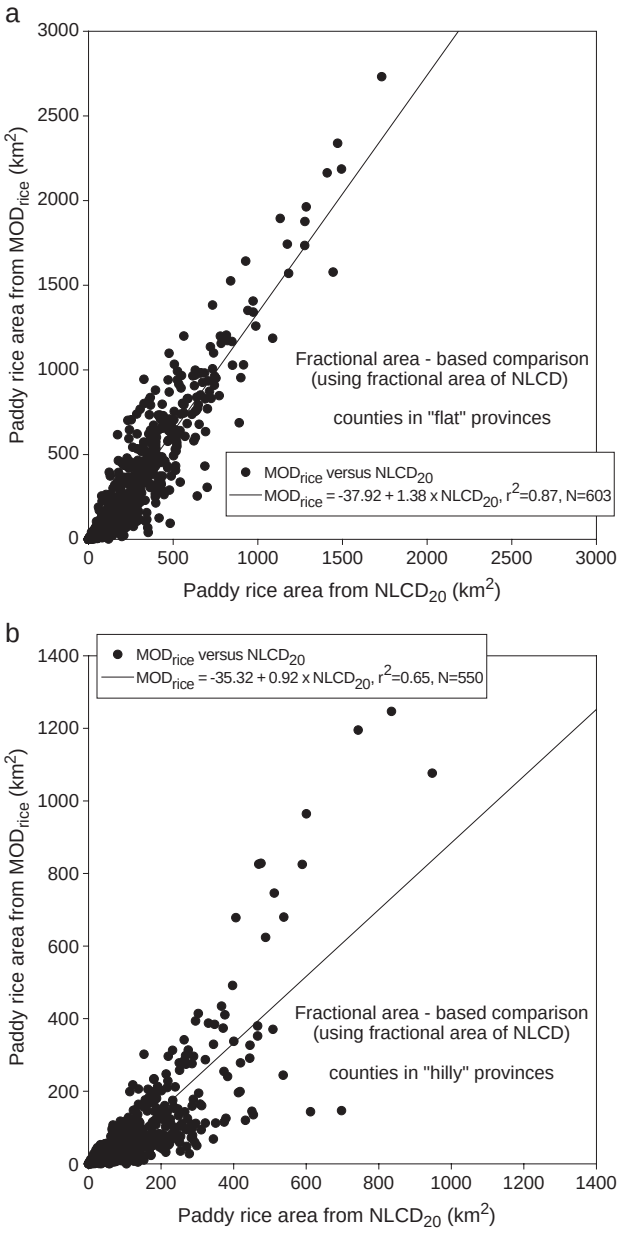

Fig. 9. County-level comparisons of area estimates of paddy rice fields in southern China between the MODIS rice algorithm (MOD_{rice}) and NLCD-2000 dataset. County-level results were analyzed using a fractional area-based comparison approach, in which we used the fractional area of paddy rice within individual pixels from the NLCD data for all MOD_{rice} pixels and $NLCD_{20}$ paddy rice pixels.

At the county level, there were also strong correlations in the area estimates of paddy rice between MOD_{rice} and $NLCD_{20}$ (Fig. 9), with RMSE=188 km^2 for flat provinces and RMSE=97 km^2 for hilly provinces. The strong relationship between the two datasets suggests that MOD_{rice} may be a useful tool to provide timely, annual rice area estimates, if a reference dataset ($NLCD_{20}$) is used to constrain the areas of analysis. The MODIS paddy rice pixels cover a total area of 250,480 km^2 (Table 3), accounting for 89% of total paddy rice area (280,555 km^2) from the NLCD database. From a standpoint of biogeochemical modeling, these results are very encouraging as biogeochemical modeling is often performed at the county scale (Li et al., 2002, 2003).

4. Discussion and summary

In this study, we used a temporal profile analysis of MODIS-derived vegetation indices to identify paddy rice fields at large spatial scales. This approach takes advantage of the flooded soils and open canopy characteristics of paddy rice fields during the phase of flooding and rice transplanting. The unique features of spectral reflectance values in that specific period make paddy rice fields separable from other croplands with no surface water (Xiao et al., 2002b). This approach is different from a number of studies that had used various clustering algorithms to identify paddy rice fields (Bachelet, 1995; Fang, 1998; Fang et al., 1998; Okamoto & Fukuhara, 1996; Van Niel et al., 2003). The previous landscape-scale study at field sites (Xiao et al., 2002b) and the results from this MODIS data analysis in southern China have demonstrated its potential for the large-scale mapping of paddy rice fields.

A number of factors could potentially affect the identification and mapping of paddy rice fields when MODIS 8-day composites are used. The first factor is related to the temporal resolution of the MOD09A1 dataset. MODIS 8-day composites are generated by selecting the date with the minimum value of blue band (the clearest atmospheric condition) within an 8-day period for each individual pixel. This compositing method could potentially omit some observations associated with the flooding/transplanting period. Use of daily MODIS data could improve the identification of the critical flooding/transplanting period, but it would require much larger datasets and would introduce a greater probability of cloud contamination. A second factor is the spatial resolution of the input datasets. Further improvements to this paddy rice detection algorithm are likely to be achieved if finer spatial resolution input data could be used. The Global Imager (GLI) sensor onboard the ADEOS II satellite (launched on December 14, 2002) offers daily images (visible, NIR and SWIR bands) at 250-m spatial resolution. When the GLI image dataset becomes publicly available, the algorithm presented in this study could be applied to GLI data and analyzed. Unfortunately, the failure of GLI sensor after its short period of operation made it impossible to have multi-year image data available to users. A third factor is residual cloud contamination in the 8-day MODIS composites. This is very important in tropical and sub-tropical areas where much of the world's rice is grown and the availability of optical satellite data is severely constrained by frequent cloud cover. Synthetic aperture radar (SAR) data is independent of meteorological conditions and, with well-timed image acquisitions, can be very effective in the mapping of paddy rice (e.g., Le Toan et al., 1997). While it is expensive to have multi-temporal SAR images at fine spatial resolution to cover large spatial domain, the temporal analysis of MODIS could help design an effective image acquisition plan of SAR images. A fourth factor is snow under the vegetation canopy that could result in higher LSWI values (Xiao et al., 2002c), which could potentially affect the study areas that experience snow events. The Land Surface Temperature (LST) product provided by the MODIS Land Science Team (Wan, 1999) could be explored for avoiding snow-covered observations, as low land surface temperature is associated with snow cover. A fifth factor is rainfall or irrigation events in other croplands or grassland, which could potentially result in situations where water-related index values are greater than or approach the greenness-related index values. A sixth factor is seasonally inundated open wetlands that could potentially be identified as rice paddies (misclassification error). Use of land cover maps at 500-m spatial resolution may help minimize the effects of the fifth and sixth factors. The MODIS Land Science Team provides a land cover dataset using MODIS data at 1-km

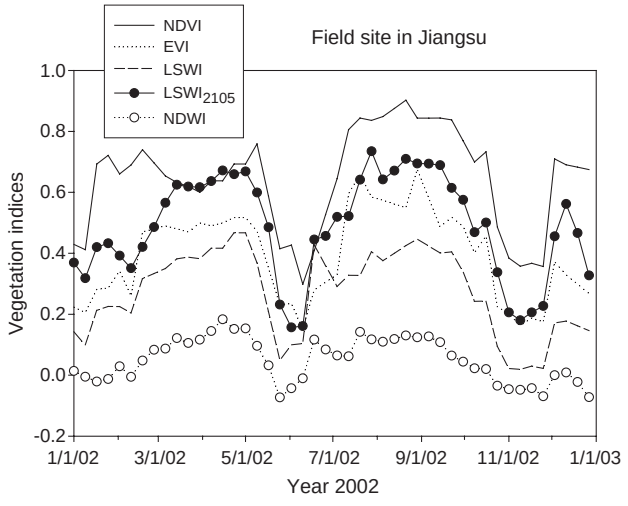

Fig. 10. A comparison of five vegetation indices in 2002 for a field site in Jiangsu province, southern China. The field site is the same as Fig. 2. This site (118°54.519′ E, 31°49.623′ N) has winter wheat crops in winter/spring seasons and paddy rice in summer/fall seasons. Harvest of winter wheat crops usually takes place in early- to mid-June, and flooding and rice transplanting usually take place in mid- to late-June (Xiao et al., 2002b).

spatial resolution (Friedl et al., 2002; Townshend, 1999), which could be useful after a thorough validation and accuracy assessment. Further effort in the MODIS-related remote sensing community should also be devoted to develop a land cover map at 500-m spatial resolution.

The MODIS sensor has three spectral bands that are sensitive to leaf water and soil moisture: NIR (NIR_2: 1230–1250 nm), and shortwave infrared ($SWIR_1$: 1628–1652 nm, $SWIR_2$: 2105–2155 nm). Following our earlier studies that used SWIR band (1580–1750 nm) of VGT sensor (Xiao et al., 2002b), we have explored MODIS $SWIR_1$ (1628–1652 nm) in this study and other studies (Xiao et al., 2004, 2005). Another water-related vegetation index is the Normalized Difference Water Index (NDWI), which can be calculated from NIR_1 (841–875 nm) and NIR_2 bands, i.e., $NDWI=(NIR_1-NIR_2)/(NIR_1+NIR_2)$ (Gao, 1996). One can also calculate a third water-related vegetation index, using NIR_1 and $SWIR_2$ bands, i.e., $LSWI_{2105}=(NIR_1-SWIR_2)/(NIR_1+SWIR_2)$. As shown in Fig. 10, all the three indices are sensitive to changes in water at the land surface during late June 2002 for a field site in Jiangling county, Jiangsu province. Although NDWI has small dynamic range (Fig. 10), additional study is needed to explore the potential of $LSWI_{2105}$ and NDWI in identifying and mapping paddy rice fields.

In summary, this study has demonstrated the potential of MODIS data and the paddy rice mapping algorithm for the large-scale mapping of paddy rice fields. This is made possible by the availability of water-sensitive shortwave infrared bands from advanced optical sensors (MODIS and VGT), which enables us to progress beyond other algorithms that are centered on leaf area index and NDVI. Our paddy rice mapping algorithm is built upon the understanding of physical system change (e.g., flooding and transplanting period) in paddy rice field, and focuses on detection of the critical phase of flooding and transplanting in paddy rice field by identifying temporary increases in a water-sensitive spectral index (LSWI). Application of this paddy rice mapping algorithm to other countries in Asia, where paddy rice agriculture dominates, could potentially provide a useful dataset of the spatial distribution of paddy rice agriculture in Asia. In addition, the algorithm can also be applied to other years of MOD09A1 data to quantify interannual variations of paddy rice fields in Asia.

Economic development in China has resulted in noticeable changes (an increase of 8 million ha) of paddy rice agriculture in China from 1995/1996 to 1999/2000 (Liu et al., 2003). Strong regional variations have been observed as southern China has experienced losses of paddy rice fields while northeastern China has had an increase of paddy rice field area (Liu et al., 2003). Changes in water management (continuous flooding versus intermittent drainage) during the past quarter century have had significant impacts on methane emissions from paddy rice fields (Li et al., 2002). Therefore, timely and accurate geospatial datasets of flooding and paddy rice fields are critically needed for quantifying the spatial pattern and temporal dynamics of methane emissions from paddy rice fields and assessing water use and food security in China and Asia.

Acknowledgement

This study is supported by grants from the NASA Terrestrial Ecology Program (NAG5-12838), the NASA Earth Observing System Interdisciplinary Science Program (NAG5-10135), and the NASA Land Cover and Land Use Change Program (NAG5-11160). We thank the three reviewers for their comments and suggestions on the earlier version of the manuscript.

References

Aselman, I., & Crutzen, P. J. (1989). Global distribution of natural freshwater wetlands and rice paddies, their net primary productivity, seasonality and possible methane emissions. *Journal of Atmospheric Chemistry*, *8*, 307–358.

Bachelet, D. (1995). Rice paddy inventory in a few provinces of China using AVHRR data. *Geocarto International*, *10*, 23–38.

Boles, S., Xiao, X., Liu, J., Zhang, Q., Munkhutya, S., Chen, S., et al. (2004). Land cover characterization of Temperate East Asia using multi-temporal image data of VEGETATION sensor. *Remote Sensing of Environment*, *90*, 477–489.

Denier Van Der Gon, H. (2000). Changes in CH_4 emission from rice fields from 1960s to 1990s: 1. Impacts of modern rice technology. *Global Biogeochemical Cycles*, *1*, 61–72.

Fang, H. (1998). Rice crop area estimation of an administrative division in China using remote sensing data. *International Journal of Remote Sensing*, *17*, 3411–3419.

Fang, H., Wu, B., Liu, H., & Xuan, H. (1998). Using NOAA AVHRR and Landsat TM to estimate rice area year-by-year. *International Journal of Remote Sensing*, *3*, 521–525.

Friedl, M. A., McIver, D. K., Hodges, J. C. F., Zhang, X. Y., Muchoney, D., Strahler, A. H., et al. (2002). Global land cover mapping from MODIS: Algorithms and early results. *Remote Sensing of Environment*, *83*, 287–302.

Frolking, S., Qiu, J. J., Boles, S., Xiao, X. M., Liu, J. Y., Zhuang, Y. H., et al. (2002). Combining remote sensing and ground census data to develop new maps of the distribution of rice agriculture in China. *Global Biogeochemical Cycles*, *16* (art. no. -1091).

Frolking, S., Xiao, X. M., Zhuang, Y. H., Salas, W., & Li, C. S. (1999). Agricultural land-use in China: A comparison of area estimates from ground-based census and satellite-borne remote sensing. *Global Ecology and Biogeography*, *8*, 407–416.

Gao, B. C. (1996). NDWI—A normalized difference water index for remote sensing of vegetation liquid water from space. *Remote Sensing of Environment*, *58*, 257–266.

Hall, D. K., Riggs, G. A., & Salomonson, V. V. (1995). Development of methods for mapping global snow cover using moderate resolution imaging spectroradiometer data. *Remote Sensing of Environment*, *54*, 127–140.

Hall, D. K., Riggs, G. A., Salomonson, V. V., DiGirolamo, N. E., & Bayr, K. J. (2002). MODIS snow-cover products. *Remote Sensing of Environment*, *83*, 181–194.

Huete, A., Didan, K., Miura, T., Rodriguez, E. P., Gao, X., & Ferreira, L. G. (2002). Overview of the radiometric and biophysical performance of the MODIS vegetation indices. *Remote Sensing of Environment*, *83*, 195–213.

Huete, A. R., Liu, H. Q., Batchily, K., & vanLeeuwen, W. (1997). A comparison of vegetation indices global set of TM images for EOS-MODIS. *Remote Sensing of Environment*, *59*, 440–451.

Huke, R. E. (1982). Rice area by type of culture: South, Southeast, and East Asia. Los Banos, Laguna, Philippines: International Rice Research Institute.

Huke, R. E., & Huke, E. H. (1997). Rice area by type of culture: South, Southeast, and East Asia, a revised and updated data base. Los Banos, Laguna, Philippines: International Rice Research Institute.

IRRI. (1993). 1993–1995 IRRI Rice Almanac. Manila: International Rice Research Institute.

Knox, J. W., Matthews, R. B., & Wassmann, R. (2000). Using a crop/soil simulation model and GIS techniques to assess methane emissions from rice fields in Asia: III. Databases. *Nutrient Cycling in Agroecosystems*, *58*, 179–199.

Leff, B., Ramankutty, N., & Foley, J. A. (2004). Geographic distribution of major crops across the world. *Global Biogeochemical Cycles*, *18*.

Le Toan, T., Ribbes, F., Wang, L., Floury, N., Ding, K., Kong, J., et al. (1997). Rice crop mapping and monitoring using ERS-1 data based on experiment and modeling results. *IEEE Transactions on Geoscience and Remote Sensing*, *1*, 41–56.

Li, C. S., Qiu, J. J., Frolking, S., Xiao, X. M., Salas, W., Moore, B., et al. (2002). Reduced methane emissions from large-scale changes in water management of China's rice paddies during 1980–2000. *Geophysical Research Letters*, *29* (art. no. -1972).

Li, C. S., Zhuang, Y. H., Frolking, S., Galloway, J., Harriss, R., Moore, B., et al. (2003). Modeling soil organic carbon change in croplands of China. *Ecological Applications*, *13*, 327–336.

Liu, J., Liu, M., Zhuang, D., Zhang, Z., & Deng, X. (2003). Study on spatial patterns of land use change in China during 1995–2000. *Science in China*, *46*, 373–384.

Maki, M., Ishiahra, M., & Tamura, M. (2004). Estimation of leaf water status to monitor the risk of forest fires by using remotely sensed data. *Remote Sensing of Environment*, *90*, 441–450.

Matthews, E., Fung, I., & Lerner, J. (1991). Methane emission from rice cultivation: Geographic and seasonal distribution of cultivated areas and emissions. *Global Biogeochemical Cycles*, *5*, 3–24.

Matthews, R. B., Wassmann, R., Knox, J. W., & Buendia, L. V. (2000). Using a crop/soil simulation model and GIS techniques to assess methane emissions from rice fields in Asia: IV. Upscaling to national levels. *Nutrient Cycling in Agroecosystems*, *58*, 201–217.

Neue, H., & Boonjawat, J. (1998). Methane emissions from rice fields. In J. Galloway, & J. Melillo (Eds.), *Asian change in the context of global climate change* (pp. 187–209). Cambridge: Cambridge University Press.

Okamoto, K., & Fukuhara, M. (1996). Estimation of paddy rice field area using the area ratio of categories in each pixel of Landsat TM. *International Journal of Remote Sensing*, *9*, 1735–1749.

Okamoto, K., & Kawashima, H. (1999). Estimating of rice-planted area in the tropical zone using a combination of optical and microwave satellite sensor data. *International Journal of Remote Sensing*, *5*, 1045–1048.

Olson, J. S. (1992). World Ecosystems (WE1.4): Digital raster data on a 10-minute geographic 1080×2160 grid. In J. J. Kineman, & M. A. Ochrenschall (Eds.), *Global ecosystems database version 1.0: Disc A, documentation manual*. Boulder, CO: US Department of Commerce/National Oceanic and Atmospheric Administration, National Geophysical Data Center.

Prather, M., & Ehhalt, D. (2001). Atmospheric chemistry and greenhouse gases. In J. T. Houghton, Y. Ding, D. J. Griggs, M. Noguer, P. J. van der Linden, X. Dai, K. Maskell, & C. A. Johnson (Eds.), *Climate change 2001: The scientific basis* (pp. 239–287). Cambridge, UK: Cambridge University Press.

Qiu, J., Tang, H., Frolking, S., Boles, S., Li, C., Xiao, X., et al. (2003). Mapping single-, double-, and triple-crop agriculture in China at 0.5°×0.5° by combining county-scale census data with a remote sensing-derived land cover map. *Geocarto International*, *18*, 3–13.

Samad, M., Merrey, D., Vermillion, D., Fuchscarsch, M., Mohtadullah, K., & Lenton, R. (1992). Irrigation management strategies for improving the performance of irrigated agriculture. *Outlook on Agriculture*, *21*, 279–286.

Tennakoon, S. B., Murty, V. V. N., & Etumnoh, A. (1992). Estimation of cropped area and grain yield of rice using remote sensing data. *International Journal of Remote Sensing*, *13*, 427–439.

Townshend, J. R. G. (1999). MODIS enhanced land cover and land cover change product: Algorithm theoretical basis document, version 2.0. 1999.

Van Niel, T. G., McVicar, T. R., Fang, H., & Liang, S. (2003). Calculating environmental moisture for per-field discrimination of rice crops. *International Journal of Remote Sensing*, *24*, 885–890.

Vermote, E. F., Vermeulen, A. (1999). Atmospheric correction algorithm: Spectral reflectance (MOD09), MODIS algorithm technical background document, version 4.0. University of Maryland, Department of Geography.

Wan, Z. (1999). MODIS Land-Surface Temperature Algorithm Theoretical Basis Document (LST ATBD) version 3.3. Institute for Computational Earth System Science, University of California, Santa Barbara.

Wassmann, R., Neue, H. U., Lantin, R. S., Makarim, K., Chareonsilp, N., Buendia, L. V., et al. (2000). Characterization of methane emissions from rice fields in Asia: II. Differences among irrigated, rainfed, and deepwater rice. *Nutrient Cycling in Agroecosystems*, *58*, 13–22.

Wilson, M. F., & Henderson-Sellers, A. (1992). A global archive of land cover and soils data for use in general circulation models. In J. J. Kineman, & M. A. Ochrenschall (Eds.), *Global ecosystems database version 1.0: Disc A, documentation manual*. Boulder, CO: US Department of Commerce, National Oceanic and Atmospheric Administration. National Geophysical Data Center.

Xiao, X., Boles, S., Frolking, S., Salas, W., Moore, B., Li, C., et al. (2002a). Landscape-scale characterization of cropland in China using Vegetation and Landsat TM images. *International Journal of Remote Sensing*, *23*, 3579–3594.

Xiao, X., Boles, S., Frolking, S., Salas, W., Moore, B., Li, C., et al. (2002b). Observation of flooding and rice transplanting of paddy rice fields at the site to landscape scales in China using VEGETATION sensor data. *International Journal of Remote Sensing*, *23*, 3009–3022.

Xiao, X., Boles, S., Liu, J., Zhuang, D., & Liu, M. (2002c). Characterization of forest types in Northeastern China, using multi-temporal SPOT-4 VEGETATION sensor data. *Remote Sensing of Environment*, *82*, 335–348.

Xiao, X., Braswell, B., Zhang, Q., Boles, S., Frolking, S., & Moore, B. (2003a). Sensitivity of vegetation indices to atmospheric aerosols: Continental-scale observations in Northern Asia. *Remote Sensing of Environment*, *84*, 385–392.

Xiao, X., He, L., Salas, W., Li, C., Moore, B., Zhao, R., et al. (2002d). Quantitative relationships between field-measured leaf area index and vegetation index derived from VEGETATION images for paddy rice fields. *International Journal of Remote Sensing*, *23*, 3595–3604.

Xiao, X., Liu, J., Zhuang, D. F., Frolking, S., Boles, S., Xu, B., et al. (2003b). Uncertainties in estimates of cropland area in China: A comparison between an AVHRR-derived dataset and a Landsat TM-derived dataset. *Global and Planetary Change*, *37*, 297–306.

Xiao, X., Zhang, Q., Braswell, B., Urbanski, S., Boles, S., Wofsy, S. C., et al. (2004). Modeling gross primary production of a deciduous broadleaf forest using satellite images and climate data. *Remote Sensing of Environment*, *91*, 256–270.

Xiao, X., Zhang, Q., Saleska, S. R., Hutyra, L., de Camargo, P. B., Wofsy, S., et al. (2005). Satellite-based modeling of gross primary production in a seasonally moist tropical evergreen forest. *Remote Sensing of Environment*, *94*, 105–122.